A Compact Model of Gate-Voltage-Dependent Quantum Effects in Short-Channel Surrounding-Gate Metal-Oxide-Semiconductor Field-Effect Transistors

Jihyun Kim, Wookyung Sun, Seunghye Park, Hyein Lim, and Hyungsoon Shin

Abstract—**In this paper, we present a compact model of gate-voltage-dependent quantum effects in short-channel surrounding-gate (SG) metal-oxide-semiconductor field-effect transistors (MOSFETs). We based the model on a two-dimensional (2-D) analytical solution of Poisson's equation using cylindrical coordinates. We used the model to investigate the electrostatic potential and current sensitivities of various gate lengths (L_g) and radii (R). Schrödinger's equation was solved analytically for a one-dimensional (1-D) quantum well to include quantum effects in the model. The model takes into account quantum effects in the inversion region of the SG MOSFET using a triangular well. We show that the new model is in excellent agreement with the device simulation results in all regions of operation.**

Index Terms—**MOSFET, gate voltage, quantum effect, short channel, surrounding gate, Poisson**

I. INTRODUCTION

As the semiconductor devices begin to enter the deep sub-micrometer regime, the short-channel effect (SCE) phenomenon will take on a more prominent role in affecting their performance. Because the SCE reduces semiconductor performance, reducing the SCE has become crucial for improving the capabilities of MOSFETs. Therefore, research on reducing the SCE is being carried out currently. In particular, attention is focused on multiple-gate MOSFETs because of their steep sub-threshold slope and low body-effect coefficient [1-13]. Among the various types of multiple-gate MOSFETs, SG MOSFETs exhibit the greatest reduction in SCE due to their excellent electrostatic-channel control [1-11]. Therefore, the results of research on SG MOSFETs should be highly helpful in permitting the realization of nanoscale device production in the future.

Although SG MOSFETs have been studied extensively, most research has been focused on long-channel [1-5]. Recently, a short-channel model for SG MOSFETs was suggested by Hamid [6]; this model maintains high accuracy even if L_g of the device is reduced down to 30 nm. However, this model involves using enormous computing power because it is based on using numerical iterations to identify individual solutions. Another short-channel model was devised by Tsormpatzoglou [9]; this model does not require using numerical iterations. However, it was developed for predicting the behavior of potential distribution along the channel only in the weak inversion region. Therefore, in this study, we tried to produce a compatible short-channel model that is accurate for all L_g and gate voltages (V_g) that does not require using numerical iterations to find solutions.

For short-channel SG MOSFETs, R of the silicon film decreases below the nanometer scale. Therefore, quantum effects must be taken into account for more precise modeling. The quantized level of quantum wells affects the distribution of electric charge. Classical

Manuscript received Jul. 26, 2011; revised Oct. 15, 2011.
Department of Electronics Engineering Ewha Womans University 11-1, Daehyun-Dong, Seodaemoon-Gu, Seoul 120-750, Korea
E-mail : hsshin@ewha.ac.kr

models assume that all of the electric charges are distributed along the conduction band, but in reality, they are located in quantized energy levels. Models that take into account these quantized levels predict a reduction of current and an increase of potential compared to classical models. For this reason, the quantum effects have been researched extensively in recent years. However, the quantum models have had too narrow a range of applications and their accuracy has been unacceptably low because the quantum effects that they encompass only apply to the threshold voltage (V_T) [11-13]. Therefore, we developed a new model that considers effectively the quantum effects for the entire range of V_g.

Using a very thin film should allow undoped devices, but in practice, SG MOSFETs are always lightly doped due to real fabrication. An approximate carrier-based compact model for SG MOSFETs with a finite doping body was developed by He [1]. The accuracy of He's model was verified by device simulation results for fully depleted SG MOSFETs for substrate doping concentration (N_{sub}) up to 10^{17} cm^{-3}. However, this model was developed for modeling long-channels so that it is not accurate for short-channel devices. Therefore, we developed an analytical and accurate drain current (I_d) model considering SCE and quantum effects within He's model. The accuracy of our model was verified by comparison with the device simulation results.

II. A MODEL FOR SHORT-CHANNEL EFFECTS

The structure of an ideal SG MOSFET as studied in this work is shown is Fig. 1 together with a cross-section profile along its cylindrical axis. For our analysis of short-channel effects, no second-order effects such as poly-silicon depletion and velocity saturation were considered for the sake of simplicity. Poisson's equation for SG MOSFETs based on the ideas presented in [6] will first be described and the potential distribution of the SG MOSFET will then be examined.

A 2-D form of Poisson's equation for considering only mobile charges was developed as follows [6]**:**

$$\nabla^2\psi(z,r)=\frac{q}{\varepsilon_{Si}}\frac{n_i^2}{N_a}e^{\frac{q(\psi-\psi_F)}{kT}} \quad (1)$$

where Ψ is the electrostatic potential, Ψ_F is the Fermi potential, and n_i is the intrinsic electron density. The potential can be written as the sum of the solution of the 1-D form of Poisson's equation for the radial direction analogous to the long-channel case and the solution for the 2-D Laplace equation, which represents the shift in the potential for the case of a short channel. This can be expressed mathematically as follows [6]:

$$\psi(z,r)=\psi_{1D}(r)+\psi_{2D}(z,r) \quad (2).$$

$\Psi_{1D}(r)$ for the 1-D potential was developed by He [1]. $\Psi_{2D}(z,r)$ for the 2-D potential is the solution to the following residual 2-D Laplace equation [6]:

$$\frac{1}{r}\frac{\partial}{\partial r}\psi_{2D}(z,r)+\frac{\partial^2}{\partial r^2}\psi_{2D}(z,r)+\frac{\partial^2}{\partial z^2}\psi_{2D}(z,r)=0 \quad (3).$$

Here, the boundary conditions are as follows:

$$\begin{aligned}\psi_{2D}(0,r)&=V_{bi}-\psi_{1D}(r)\\ \psi_{2D}(L_g,r)&=V_{bi}+V_d-\psi_{1D}(r)\end{aligned} \quad (4).$$

For these two equations, V_{bi} is the built-in potential, and V_d is the drain voltage.

Previous investigations have used a disjunction of variables to solve Eq. (3) [6-8]. However, this requires the use of more complex mathematical formulae, and therefore, in our study, we assumed that $\Psi_{2D}(z,r)$ took on a parabolic dependence in terms of the position in the

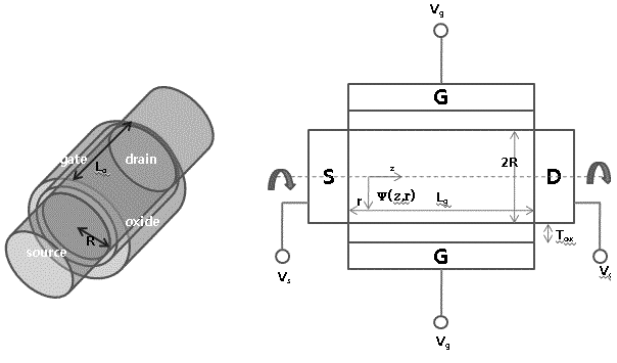

(a) (b)

Fig. 1. Schematic of (a) the 3-D structure of a SG MOSFET and (b) a cross-section profile along its cylindrical axis.

silicon film as shown below:

$$\psi_{2D}(z,r) = C_0(z) + C_1(z)r + C_2(z)r^2 \quad (5).$$

Because SG MOSFETs are symmetric, $C_1(z)$ is written as follows:

$$\frac{\partial}{\partial r}\psi_{2D}(z,r)\bigg|_{r=0} = C_1(z) = 0 \quad (6).$$

When applying only a 2-D potential to the Gauss law, the result is as follows:

$$C_{ox}\psi_{2D}(z,r) = -\varepsilon_{si}\frac{\partial\psi_{2D}(z,r)}{\partial r}\bigg|_{r=R} \quad (7)$$

and

$$C_2(z) = -\frac{C_{ox}}{C_{ox}R^2 + 2\varepsilon_{si}R}C_0(z) \quad (8).$$

From Eq. (6, 8), $\Psi_{2D}(z,r)$ can be written as

$$\psi_{2D}(z,r) = C_0(z) - \frac{C_{ox}}{C_{ox}R^2 + 2\varepsilon_{si}R}C_0(z)r^2 \quad (9).$$

If we apply Eq. (9) to Eq. (3), the result is as follows:

$$\lambda^2\frac{\partial^2}{\partial z^2}C_0(z) - C_0(z) = 0 \quad (10)$$

and

$$\lambda = \sqrt{\frac{\varepsilon_{OX}\left(R^2 - r^2\right) + 2\varepsilon_{si}R^2\ln\left(1 + \frac{t_{OX}}{R}\right)}{4\varepsilon_{OX}}} \quad (11).$$

The solution to Eq. (10) is written below:

$$C_0(z) = Ae^{\frac{z}{\lambda}} + Be^{-\frac{z}{\lambda}} \quad (12).$$

Using the boundary conditions shown in Eq. (4) yields the following:

$$\begin{aligned} C_0(0) &= V_{bi} - \psi_{1D}(0) \\ C_0(L_g) &= V_{bi} + V_d - \psi_{1D}(0) \end{aligned} \quad (13).$$

From Eq. (12, 13), A and B can be isolated as follows:

$$A = -\frac{C_0(0)e^{-\frac{L_g}{\lambda}} - C_0(L_g)}{e^{\frac{L_g}{\lambda}} - e^{-\frac{L_g}{\lambda}}} \quad (14)$$

and

$$B = \frac{C_0(0)e^{\frac{L_g}{\lambda}} - C_0(L_g)}{e^{\frac{L_g}{\lambda}} - e^{-\frac{L_g}{\lambda}}} \quad (15).$$

Subsequently, from Eq. (9, 12, 14, 15), $\Psi_{2D}(z,r)$ can be written as follows:

$$\psi_{2D}(z,r) = \left[C_0(0)\left\{\frac{\sinh\left(\frac{L_g - z}{\lambda}\right)}{\sinh\left(\frac{L_g}{\lambda}\right)}\right\} + C_0(L_g)\left\{\frac{\sinh\left(\frac{z}{\lambda}\right)}{\sinh\left(\frac{L_g}{\lambda}\right)}\right\}\right]\cdot\left\{1 - \frac{C_{OX}r^2}{C_{OX}R^2 + 2\varepsilon_{Si}R}\right\} \quad (16).$$

The barrier height of a short-channel device is determined by the minimum 2-D potential. The potential along the longitudinal direction can be calculated where the differentiated form of Eq. (16) is equal to zero:

$$\psi_{2D}(z,r)_{\min} = \frac{\sqrt{-\left\{C_0(0)^2 + C_0(L_g)^2\right\} + 2C_0(0)C_0(L_g)\cosh\left(\frac{L_g}{\lambda}\right)}}{\sinh\left(\frac{L_g}{\lambda}\right)} \quad (17).$$

When L_g is large, Eq. (17) can be simplified as follows:

$$\psi_{2D}(z,r)_{\min} = 2\sqrt{C_0(0)C_0(L_g)}e^{-\frac{L_g}{2\lambda}} \quad (18).$$

The potential reduces to $\psi(z,r) \approx \psi_{1D}(r)$ because

Eq. (18) is almost zero for large L_g. Therefore, the increase in potential for a short-channel device, $\Delta\psi(z,r)$, is given by:

$$\therefore \Delta\psi(z,r) = \psi_{2D}(z,r)_{\min} \quad (19).$$

An analytical current equation can be derived from the Pao-Sah current equation using a gradual channel approximation and an integration term as detailed below [1]:

$$I_{ds} = \mu \frac{W}{L_g}\int_0^{V_d} q_I dV = \frac{4\pi\mu\varepsilon_{si}}{L_g}\left(\frac{2q}{kT}\right)^2 f(n_0)\Big|_{n_{0d}}^{n_{0s}} \quad (20)$$

$$\begin{aligned} f(n_0) &= \frac{1}{2}\ln\left[1-\frac{R^2q^2N_a}{8\varepsilon_{si}kT}\frac{n_0}{N_a}\right] \\ &+ \frac{\left[\varepsilon_{ox}-2\varepsilon_{si}\ln\left(1+\frac{t_{ox}}{R}\right)\right]}{\varepsilon_{ox}\left[1-\frac{R^2q^2N_a}{8\varepsilon_{si}kT}\frac{n_0}{N_a}\right]} + \frac{\varepsilon_{si}\ln\left(1+\frac{t_{ox}}{R}\right)}{\varepsilon_{ox}\left[1-\frac{R^2q^2N_a}{8\varepsilon_{si}kT}\frac{n_0}{N_a}\right]^2} \\ &+ \frac{q}{2kT}\left(\sqrt{\frac{qN_aR^2}{16\varepsilon_{si}}}+\frac{\sqrt{2q\varepsilon_{si}N_a}}{C_{ox}}\right)\sqrt{\frac{qN_aR^2}{64\varepsilon_{si}}-\frac{2kT}{q}\ln\left[1-\frac{R^2q^2N_a}{8\varepsilon_{si}kT}\frac{n_0}{N_a}\right]} \end{aligned} \quad (21)$$

and

$$n_0 = \frac{n_i^2}{N_a}\exp\frac{q\left(V_g-\Delta\psi(z,r)-V_{FB}-\left[\sqrt{\frac{qN_aR^2}{64\varepsilon_{si}}-\frac{2kT}{q}\ln\left[1-\frac{R^2q^2N_a}{8\varepsilon_{si}kT}\frac{n_0}{N_a}\right]}+\sqrt{\frac{qN_aR^2}{64\varepsilon_{si}}}\right]^2-\frac{Q}{C_{ox}}-\psi_F\right)}{kT} \quad (22)$$

where μ is the effective mobility, W is the channel width, V_{FB} is the flat band voltage, and Q is the total charge density.

The lightly doped short-channel SG MOSFET characteristics for all operating regions can be predicted using this approximated yet continuous analytical model. To test our model, we assumed that the gate substances were mid-gap metals so that the work function difference (ΔΦ) was 0 V for comparison. A constant mobility of 400 $cm^2 \cdot Vs^{-1}$ was used for all calculations and simulations. Fig. 2 shows a comparison of the I_d versus V_g for different N_{sub} compared with the results for device simulation. From the results, it is evident that the new model is more accurate in comparison to the old model.

Fig. 3 shows the center potential distribution along a channel for different V_g. It can be seen that the potential

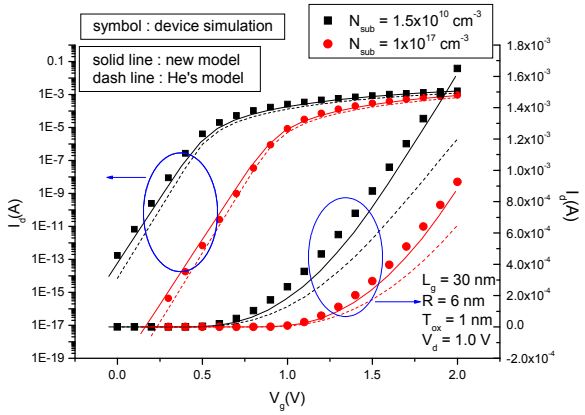

Fig. 2. Differences in currents between results for the device simulation (ATLAS) and for analytical models. The solid line denotes the results of the new model that was developed in this study and the dashed line denotes the results for the long-channel model that was developed by He [1]. The symbols show the results for the device simulation.

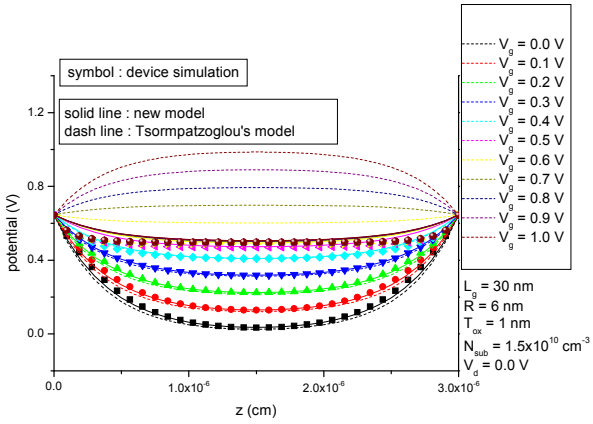

Fig. 3. A comparison of the electrostatic potential between the device simulation and numerical models. The solid line represents the results of the new model that was developed in this study and the dashed line represents the results for the short-channel model developed by Tsormpatzoglou [9]. The symbols show the results for the device simulation.

predicted by the new model shows a gradual saturation trend for all operating regions, while Tsormpatzoglou's model does not reflect potential saturation phenomena. Moreover, high accuracy on the source and drain sides is important for short-channels. As shown in Fig. 3, as it approaches the source and drain sides, the new model proves to be more superior in accuracy.

As seen in Fig. 4, the SG MOSFET current predicted by the new model matches well with that obtained by the device simulation from the sub-threshold region to the inversion region even for ultra-small devices such as

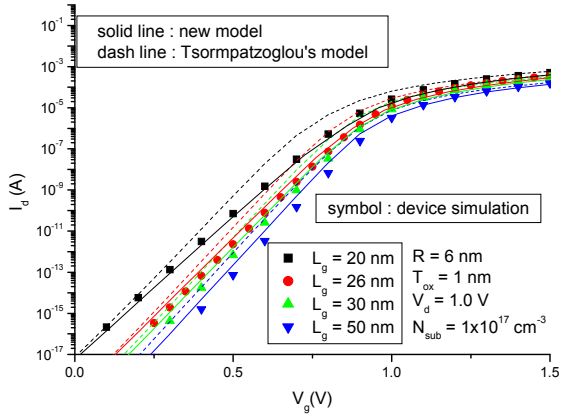

Fig. 4. A comparison of I_d versus V_g between the results for the analytical models (lines) and those for the device simulation (symbols) for different L_g.

where L_g = 20 nm. However, Tsormpatzoglou's model in the sub-threshold region has an increased deviation from the device simulation for L_g = 20 nm.

III. A Model for Quantum Effects

Models that take into account quantum effects have so far been able to resolve the changes of potential only at V_T [11-13]. However, because quantum effects appear in different ways depending on the degree of inversion, changes in the potential well over a range of V_g values must be taken into account. For the energy–band profile across the channel, two different cases, the sub-threshold region and inversion region, should be considered. For the sub-threshold region, the potential profile in the channel is almost flat (Fig. 5 (a)) and the band diagram is close to a rectangular well (structural confinement). In this case, the quantum effect caused by structural confinement is negligible if the R of the SG MOSFET is larger than 5 nm. In contrast, the potential profile around the Si/SiO_2 interface is close to the shape of a triangular well for the inversion region (Fig. 5(b)), and therefore, the quantum effect due to triangular well should be considered (electronic confinement). The accuracy of the model can be increased by examining this phenomenon for a range of V_g values because the quantum well appears in different forms according to V_g.

A plot of the electron energy level versus V_g characteristics obtained by solving Schrödinger's equation is shown in Fig. 6 for various R. In the sub-threshold region (V_g < 0.5 V), $E_{c\_surface}$, E_{c_center}, and $E_{QM,1}$

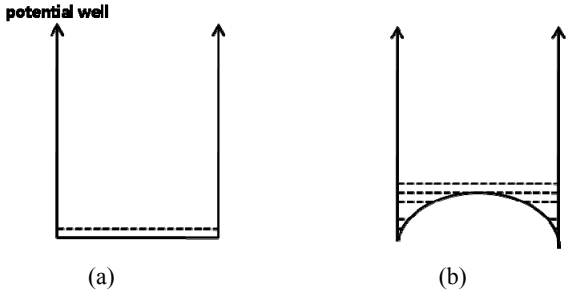

Fig. 5. Changes in the quantum well (a) in the sub-threshold region and (b) in the inversion region.

are almost the same. This indicates that the potential is almost flat and the quantum effect can be neglected. However, in the inversion region (V_g > 0.5 V), the energy bands starts to bend (E_{c_center} is higher than $E_{c\_surface}$), and $E_{QM,1}$ is located between $E_{c\_surface}$ and E_{c_center}. The difference between $E_{c\_surface}$ and $E_{QM,1}$ increases with increasing V_g, which reveals that the quantum effect is dependent on V_g. According to these phenomena, the new model takes into account the quantum effects with dependence on V_g using a triangular well and the quantum effects are neglected in the sub-threshold region for simplification.

For the quantum case, the sheet density of the carriers can be determined from the following equation [13]:

$$Q = \frac{qkT}{\pi\hbar^2}\sum_j g_j m_j^{DOS}\sum_i \exp\left(\frac{E_F - \left(\frac{E_g}{2} - q\psi_s^{QM} + E_{ij}\right)}{kT}\right) \quad (23)$$

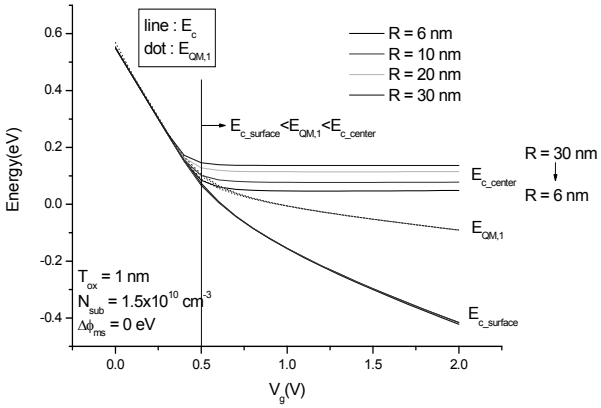

Fig. 6. Electron energy levels of the conduction band at Si/SiO_2 interfaces ($E_{c\_surface}$), the center (E_{c_center}), and the first quantization level ($E_{QM,1}$) vs. V_g characteristics of a SG MOSFET with various R.

where ħ is Planck's constant, i is the index of the sub-band, j is the index of the valley, g_i is the valley degeneracy, m_j^{DOS} is the density of the state effective mass, E_F is the Fermi level, E_g is the energy gap, Ψ_s^{QM} is the potential of the quantum case, and E_{ij} is the Eigen energy.

The ways by which E_{ij} can be determined are categorized into two cases depending on the form of the energy well on the band diagram, which can be rectangular or triangular [12]. Existing quantum models take into account quantum effects only at V_T using a rectangular well [11-13]. However, as we detailed above, the quantum effects for the sub-threshold region can be ignored and the influence of the quantum effects increases in the inversion region. Therefore, our model can be used to take into account the quantum effect by identifying the energy level in the inversion region.

Due to the band bending phenomenon in the inversion region, we used an energy level equation for a triangular potential well as follows [14]:

$$E_{ij} = \left[\frac{3}{2}\pi\left(i-\frac{1}{4}\right)\right]^{\frac{2}{3}}\left[\frac{\left(q\xi_{eff}\hbar\right)^2}{2m_j}\right]^{\frac{1}{3}} \quad (24)$$

where ξ_{eff} is the effective electric field and m_j is the electron effective mass in the j^{th} valley. For the energy level presented in Eq. (24), better consensus is reached with the self-constant calculation results when using ξ_{eff} instead of the electric field at the surface ξ_s under the inversion condition [15, 16]. The effective electric field can be written as follows:

$$\xi_{eff} = \frac{1}{\varepsilon_{si}}\left(\eta Q_{inv} + Q_{D,\max}\right) \quad (25)$$

where η is a fitting parameter, ε_{si} is the permittivity, Q_{inv} is the inversion sheet charge density and $Q_{D,max}$ is the maximum depletion sheet charge density. The parameter η depends on the orientation of the crystal surface and can be assumed to take on values different from 1/2 due to the effects of valley repopulation [15]. For estimating the electron mobility on the (110)- and (111)-oriented surfaces, η = 1/3 can be assumed [15, 17]. In addition, η = 1/2 can be assumed for a (100)-oriented surface. Substituting Eq. (24) in Eq. (23) yields Ψ_s^{QM} as detailed below:

$$\psi_s^{QM} = \frac{kT}{q}\ln\left(\frac{\frac{\pi\hbar^2}{qkT}Q\exp\left(\frac{E_g/2-E_F}{kT}\right)}{\sum_j g_j m_j^{DOS}\sum_i \exp\left(-\left[\frac{3\pi}{2}\left(i-\frac{1}{4}\right)\right]^{\frac{2}{3}}\left[\frac{\left(q\xi_{eff}\hbar\right)^2}{2m_j}\right]^{\frac{1}{3}}\frac{1}{kT}\right)}\right) \quad (26).$$

The potential shift in quantum ($\Delta\Psi_s^{QM}$) is as follows:

$$\Delta\Psi_s^{QM} = \Psi_s^{QM} - \Psi_s^{CL} \quad (27)$$

where Ψ_s^{CL} is the potential for the classical model. To include quantum effects, $\Delta\Psi_s^{QM}$ values at the source ($\Delta\Psi_s^{QM,S}$) and drain ($\Delta\Psi_s^{QM,D}$) are calculated for each Q using Eq. (27). The average of $\Delta\Psi_s^{QM}$ ($\Delta\Psi_s^{QM,avg}$) is adopted in our model as shown below:

$$\Delta\Psi_s^{QM,avg} = \frac{\Delta\Psi_s^{QM,S} + \Delta\Psi_s^{QM,D}}{2} \quad (28).$$

When considering the quantum effects, Eq. (28) is applied to Eq. (22) as follows:

$$n_0 = \frac{n_i^2}{N_a}\exp\frac{q\left(V_g + \Delta\Psi_s^{QM,avg} - \Delta\psi(z,r) - V_{FB} - \left[\sqrt{\frac{qN_aR^2}{64\varepsilon_{si}}} - \frac{2kT}{q}\ln\left[1-\frac{R^2q^2N_a}{8\varepsilon_{si}kT}\frac{n_0}{N_a}\right]\right] + \sqrt{\frac{qN_aR^2}{64\varepsilon_{si}}}^2 - \frac{Q}{C_{ox}} - \psi_F\right)}{kT} \quad (29).$$

To test our quantum model, the first sub-band of two-fold degeneracy is considered for all calculations because most of the carriers are positioned in the lowest band, which is the first sub-band with two-fold degeneracy. As the (100)-orientation is taken as the basic condition, η = 1/2 is used.

$\Delta\Psi_s^{QM,avg}$ versus V_g for the old and new models are compared with various V_d, as shown in Fig. 7. Because the old model takes into account the quantum effects only at V_T with a rectangular well, there is no difference in V_g. In comparison, $\Delta\Psi_s^{QM,avg}$ is calculated for each Q at different V_g and V_d in the new model. $\Delta\Psi_s^{QM,avg}$ increases with increasing V_g and decreasing V_d when the shape of the triangular well becomes sharper.

Fig. 8 shows a comparison between the results for device simulation and analytical models for different N_{sub} and R. The old model fails to reflect the decrease in the current in the inversion region. Because $\Delta\Psi_s^{QM,avg}$ is too

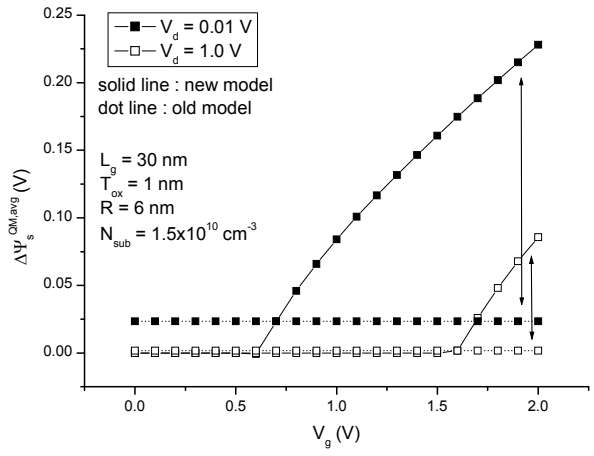

Fig. 7. $\Delta\Psi_s^{QM,avg}$ for the old model (dot line) and for new model (solid line) with various V_d. The solid symbol represents the results for V_d=0.01 V and the open symbol represents the results for V_d=1.0 V.

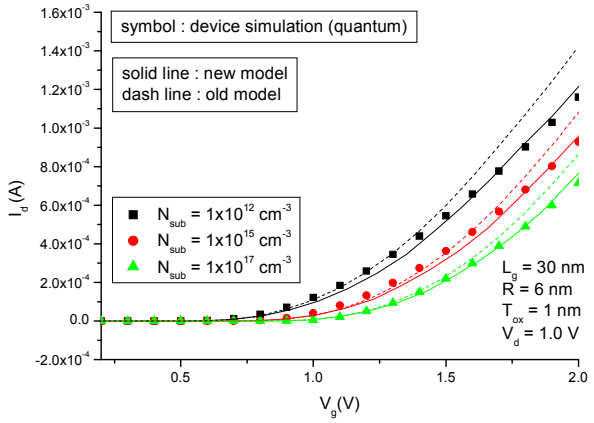

(a)

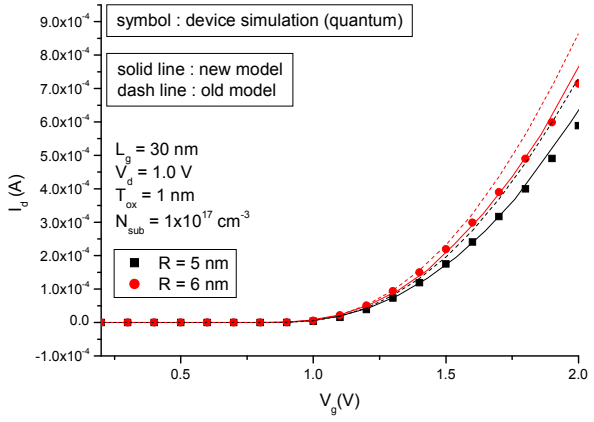

(b)

Fig. 8. A comparison of the accuracy of I_d vs. V_g for the old model (dash line) and new model (solid line) for different, (a) N_{sub} and (b) R. The symbols show the results for the device simulation.

small at V_T, the old model overestimates the current in the inversion region. In comparison, new model has superior accuracy even when N_{sub} increases to 1×10^{17} cm^{-3} and R decreases to 5 nm. Furthermore, the new model has excellent accuracy for SG MOSFETs with various L_g, V_d, and T_{ox} (not shown here).

IV. CONCLUSIONS

In summary, we derived a compact model for short-channel SG MOSFETs by considering V_g-dependent quantum effects. We extended the compact model of He to study short-channel SG MOSFETs. By solving a 2-D Poisson equation, we assumed a parabolic 2-D potential approximation for all V_g without carrying out numerical iterations. By including the SCE within the existing long-channel I_d model, our new model describes with good accuracy the output characteristics for short-channel SG MOSFETs. In addition, we present an analytical model for $\Delta\Psi_s^{QM,avg}$ due to quantum confinement in SG MOSFETs. To enhance the accuracy of our model, we considered the V_g dependence of the quantum effects in the inversion region. A numerical simulation was performed to confirm the validity of our simplification and the analytical solution to our model. The I-V characteristics of the model were compared with device simulation results. Finally, the new model shows substantially better accuracy than the existing model in short-channel.

ACKNOWLEDGMENTS

This research was supported by Basic Science Research Program through the National Research Foundation of Korea (NRF) funded by the Ministry of Education, Science and Technology (grant number: 2010-0007016)

REFERENCES

[1] J. He, F. Liu, W. Bian, J. Feng, J. Zhang and X. Zhang, "An approximate carrier-based compact model for fully depleted surrounding-gate MOSFETs with a finite doping body," *Semicond. Sci. and Technol.,* Vol.22, No.6, pp.671-677, 2007.

[2] A. Son, J. Kim, N. Jeong, J. Choi and H. Shin,

"Improved Explicit current-Voltage Model for Long-Channel Undoped Surrounding-Gate Metal Oxide Semiconductor Field Effect Transistor," *J. J. Appl. Phys.,* Vol.48, pp.412-413, 2009.

[3] Y. Chen and J. Luo, "A Comparative Study of Double-Gate and Surrounding-Gate MOSFETs in Strong Inversion and Accumulation Using An Analytical Model," *Proc. Int. Conf. Modeling Simulation of Microsystems*, Vol.1, pp.546-549, 2001.

[4] D. Jimenez and B. Inguiez, "Continuous analytic I-V model for surrounding-gate MOSFETs," *IEEE Electron Device Lett.*, Vol.25, No.8, pp.571-573, 2004.

[5] B. Iniguez, D. Jimenez, J. Roig, H.-A. Hamidi, L. F. Marsal and J. Pallares, "Explicit continuous model for long-channel undoped surrounding-gate MOSFETs," *IEEE Trans. Electron. Devices*, Vol.52, No.8, pp.1868-1873, 2005.

[6] H. A. E. Hamid, B. Iniguez and J. R. Guitart, "Analytical Model of the Threshold Voltage and Subthreshold Swing of Undoped Cylindrical Gate-All-Around-Based MOSFETs," *IEEE Electron Device*, Vol.54, No.3, pp.572-579, 2007.

[7] A. Aouaj, A. Bouziane and A. Nouacry, "Analytical 2D modelling for potential distribution and threshold voltage of the short channel fully depleted cylindrical/surrounding gate MOSFET", *International Journal of Electronics*, Vol.92, No.8, pp.437-443, 2005.

[8] C. Suh, "Two-Dimensional Analytical Model for Deriving the Threshold Voltage of a Short Channel Fully Depleted Cylindrical/Surrounding Gate MOSFET," *J. Semi. Tech. and Sci.*, Vol.11, No.2, pp.111-120, 2011.

[9] A. Tsormpatzoglou, D. H. Tassis, C. A. Dimitriadis, G. Ghibaudo, G. Pananakakis and R. Clerc, "A compact drain current model of short-channel cylindrical gate-all-around MOSFETs," *Semicond. Sci. Technol*., Vol.24, No.7, pp.075017, 2009.

[10] A. Kranti, S. Haldar, R. S. Gupta, "Analytical model for threshold voltage and I-V characteristics of fully depleted short channel cylindrical/ surrounding gate MOSFET", Microelectronic Engineering, Vol.56, No.3-4. , pp.241-259, 2001.

[11] Y. Yuan, B. Yu, J. Song and Y. Taur, "An analytic model for threshold voltage shift due to quantum confinement in surrounding gate MOSFETs with anisotropic effective mass", *Solid State elec.*, Vol.53, No.2, pp.140-144, 2009.

[12] J.L. Autran, D. Munteanu, O. Tintori, S. Harrison, E. Decarre and T. Skotnicki, "Quantum-Mechanical Analytical Modeling of Threshold Voltage in Long-Channel Double-Gate MOSFET with Symmetric and Asymmetric Gates," *NSTI nanotech*, Vol.2, pp.163-166, 2004.

[13] S. Mohammadi and A. Afzali-Kusha, " A Surface Field Based Model for Ultra Thin Body Undoped Symmetric DG MOSFETs," *10th IEEE Int. Conf. on ULIS,* pp.357-361, Mar., 2009.

[14] J. Davies (1998), *The physics of low dimensional semiconductors: an Introduction*, Cambridge University Press.

[15] K. Lee, J. Choi, S. Sim and C. Kim, "Physical Understanding of Low-Field Carrier Mobility in Silicon MOSFET Inversion Layer," *IEEE Trans. Electron. Devices*, Vol.38, No.8, pp.1905-1912, 1991.

[16] F. Stern, "Self-Consistent Result for n-type Si Inversion Layer," *Phys. Review B*, Vol.5, No.12, pp.4891-4899, 1972.

[17] S. Takagi, A. Toriumi, M. Iwase and H. Tango, "On the Universality of Inversion Layer Mobility in Si MOSFET's: Part Ⅱ- Effects of Surface Orientation," *IEEE Trans. Electron. Devices*, Vol.41, No.12, pp.2363-2368, 1994.

Jihyun Kim received the B.S. and the M.S. degrees in electronics engineering from EWHA Womans University, Seoul, Korea, in 2005 and 2007, respectively, where she is currently working toward the Ph. D. degree. Her major interest is 3D device analysis and modeling.

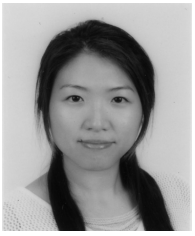

Wookyung Sun received the B.S. and the M.S. degrees in electronics engineering from EWHA Womans University, Seoul, Korea, in 1999 and 2001, respectively.

From 2001 to 2009, she was with Hynix Company, Ltd., in Korea, where she was engaged in research on the development of DRAM memory. She is currently working toward the Ph.D. degree in electronics engineering from EWHA Womans University, Seoul, Korea. Her major interest is Si based device's reliability.

Seunghye Park received the B.S. degree in electronics engineering from EWHA Womans University, Seoul, Korea, in 2010, where she is currently working toward the M.S degree. Her major interest is mobility and modeling and analysis of SG and DG Silicon device.

Hyein Lim received the B.S. degree in electronics engineering from EWHA Womans University, Seoul, Korea, in 2010, where she is currently working toward the M.S. degree. Her major interest is circuit developments and modeling based on Si.

Hyungsoon Shin received the B.S. degree in electronics engineering from Seoul National University, Seoul, Korea, in 1982, and the M.S. and Ph.D. degrees in electrical engineering from the University of Texas at Austin, Austin, in 1984 and 1990, respectively.

From 1990 to 1994, he was with LG Semicon Company, Ltd., in Korea, where he was engaged in research on the development of DRAM, SRAM, and Flash memory. Since 1995, he has been with the Department of Electronics Engineering, EWHA Womans University, Seoul. His current research interests include new processes, devices, and circuit developments and modeling based on Si, both for high-density memory and RF ICs.